nature nanotechnology

LETTERS

https://doi.org/10.1038/s41565-018-0161-8

Continuous-wave upconverting nanoparticle microlasers

Angel Fernandez-Bravo[1], Kaiyuan Yao[1,2], Edward S. Barnard[1], Nicholas J. Borys[1], Elizabeth S. Levy[1], Bining Tian[1], Cheryl A. Tajon[1], Luca Moretti[3], M. Virginia Altoe[1], Shaul Aloni[1], Kenes Beketayev[4], Francesco Scotognella[3,5], Bruce E. Cohen[1*], Emory M. Chan[1*] and P. James Schuck[1,6*]

Reducing the size of lasers to microscale dimensions enables new technologies[1] that are specifically tailored for operation in confined spaces ranging from ultra-high-speed microprocessors[2] to live brain tissue[3]. However, reduced cavity sizes increase optical losses and require greater input powers to reach lasing thresholds. Multiphoton-pumped lasers[4–7] that have been miniaturized using nanomaterials such as lanthanide-doped upconverting nanoparticles (UCNPs)[8] as lasing media require high pump intensities to achieve ultraviolet and visible emission and therefore operate under pulsed excitation schemes. Here, we make use of the recently described energy-looping excitation mechanism in Tm^{3+}-doped UCNPs[9] to achieve continuous-wave upconverted lasing action in stand-alone microcavities at excitation fluences as low as 14 kW cm^{-2}. Continuous-wave lasing is uninterrupted, maximizing signal and enabling modulation of optical interactions[10]. By coupling energy-looping nanoparticles to whispering-gallery modes of polystyrene microspheres, we induce stable lasing for more than 5 h at blue and near-infrared wavelengths simultaneously. These microcavities are excited in the biologically transmissive second near-infrared (NIR-II) window and are small enough to be embedded in organisms, tissues or devices. The ability to produce continuous-wave lasing in microcavities immersed in blood serum highlights practical applications of these microscale lasers for sensing and illumination in complex biological environments.

Upconversion occurs in lanthanide-doped materials[11–13] through the step-wise absorption of multiple photons. Because upconversion is orders of magnitude more efficient than standard nonlinear optical processes such as two-photon absorption[14], lanthanide-doped systems emerged as promising gain media for the production of visible-wavelength coherent radiation from near-infrared (NIR) excitation[15]. To achieve the population inversion required for lasing, upconverting lasers still require high pump intensities (approximately 10^7–10^{10} W cm^{-2}; Fig. 1a) that constrain the gain media and the operating conditions used for such systems. Commonly, upconverting lasers are assembled from metre-long doped glass fibres to distribute and dissipate heat generated by high pump intensities. To maintain the high excited-state populations required for upconversion, these delicate fibres are drawn from low-phonon-energy metal fluoride glasses (such as ZBLAN) that have size and geometric limitations as well as strict processing requirements[16,17].

The use of UCNPs for upconverting lasers offers an avenue for fully solution-processed, bottom-up microlaser production, which in turn enables simple fabrication and assembly into a wide variety of photonic structures and device platforms[10]. These solution-processed upconverting lasers can be produced from biologically compatible materials by control of UCNP surface properties[8,18]. However, a considerable obstacle to the adoption of UCNP-based lasers has been the requirement for pulsed excitation[7] to avoid optical and thermal damage associated with intense continuous-wave (CW) excitation, a problem compounded by heat-induced increases in lasing thresholds. UCNPs exploiting an avalanche-like energy-looping mechanism[9] can bypass these issues, resulting in solution-processed, bio-integrable CW upconverting microlasers.

We have designed laser microcavities to incorporate three technical innovations intended to lower upconverting lasing thresholds. First, the cavities are fabricated from polystyrene microspheres (diameter 5 μm) that are known to host whispering-gallery modes[19] (WGMs), closed-loop light paths that are guided by total internal reflection within the microsphere surface (Fig. 1b). Previously, the use of WGMs in larger microspheres of bulk upconverting material has led to low-power lasing[20]. The 5 μm polystyrene cavities used in this work support both transverse electric and transverse magnetic propagating modes with high quality factors (Q), and the number and wavelength of the amplified modes can be selected by modulating the diameter of the microspheres. Additionally, polymers are attractive cavity materials for biological lasing applications because monodisperse libraries can readily be fabricated from biocompatible or biodegradable materials. One main limitation is that some organic polymers have been shown to degrade at the temperatures reached under sustained CW excitation[21].

To minimize the thermal degradation of the cavity materials, the second innovation that we incorporate is the use of Tm^{3+}-doped energy-looping nanoparticles (ELNPs)[9] as gain media in these WGM microresonators. When excited non-resonantly at 1,064 nm, ELNPs exhibit upconverted luminescence with characteristic blue and NIR Tm^{3+} emission peaks (Supplementary Fig. 1). The 1,064-nm light used to excite ELNPs reduces the thermal load of the gain medium, because the ELNP host matrix, $NaYF_4$, and the polystyrene cavity both absorb less at 1,064 nm than at 980 nm, which is used to excite nearly all other UCNP lasers. Additionally, 1,064 nm falls within the NIR-II window of photon energies that transmit efficiently through tissue. Most importantly, the ELNPs upconvert the 1,064-nm light to visible and NIR light using an avalanche-like

[1]The Molecular Foundry, Lawrence Berkeley National Laboratory, Berkeley, CA, USA. [2]Department of Mechanical Engineering, UC Berkeley, Berkeley, CA, USA. [3]Department of Physics, Politecnico di Milano, Milan, Italy. [4]Computer Science Laboratory, National Laboratory Astana, Astana, Kazakhstan. [5]Center for Nano Science and Technology@PoliMi, Istituto Italiano di Tecnologia, Milan, Italy. [6]Department of Mechanical Engineering, Columbia University, New York, NY, USA. *e-mail: becohen@lbl.gov; emchan@lbl.gov; p.j.schuck@columbia.edu

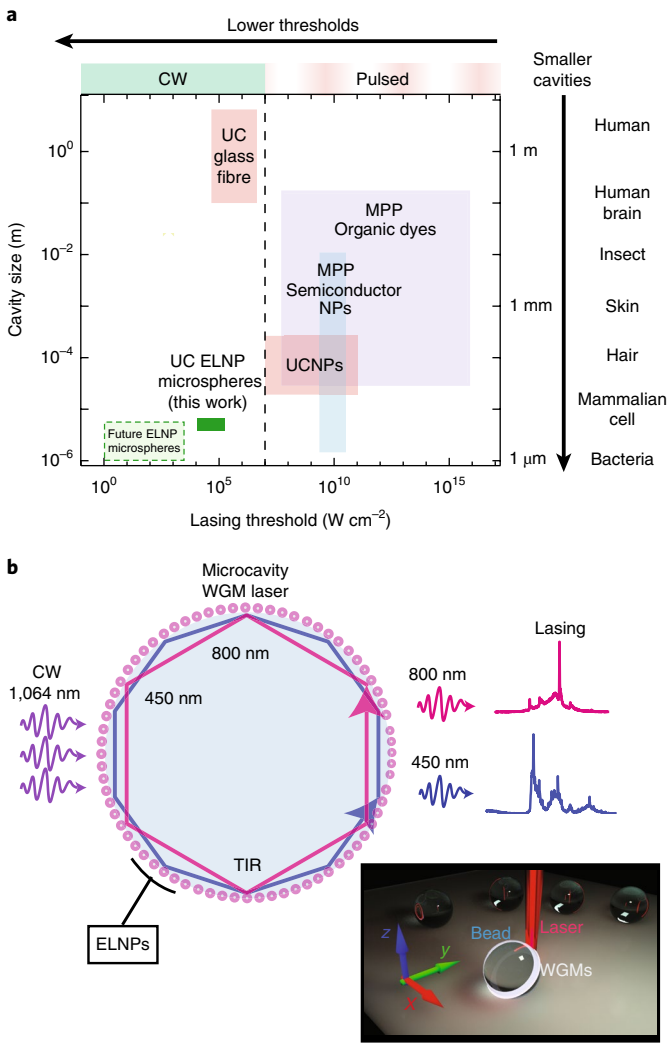

Fig. 1 | Use of microsphere cavity modes and ELNPs for achieving CW, upconverting lasing at low powers. a, Graphical comparison of lasing thresholds and cavity size between our microcavities and other upconverting (UC) systems[5,6,16,29–31] and multiphoton-pumped (MPP) architectures[7,32–35]. Thresholds for pulsed experiments represent peak power densities. Thresholds extrapolated for future microsphere devices reflect likely improvements in input coupling (such as waveguide coupling) and UCNP composition (for example, exploiting high lanthanide doping and heterostructuring)[14]. NPs, nanoparticles. **b**, Schematic of excitation and lasing in ELNP-coated microbeads. TIR, total internal reflection. Inset: 3D schematic depicting lasing WGMs in a microsphere.

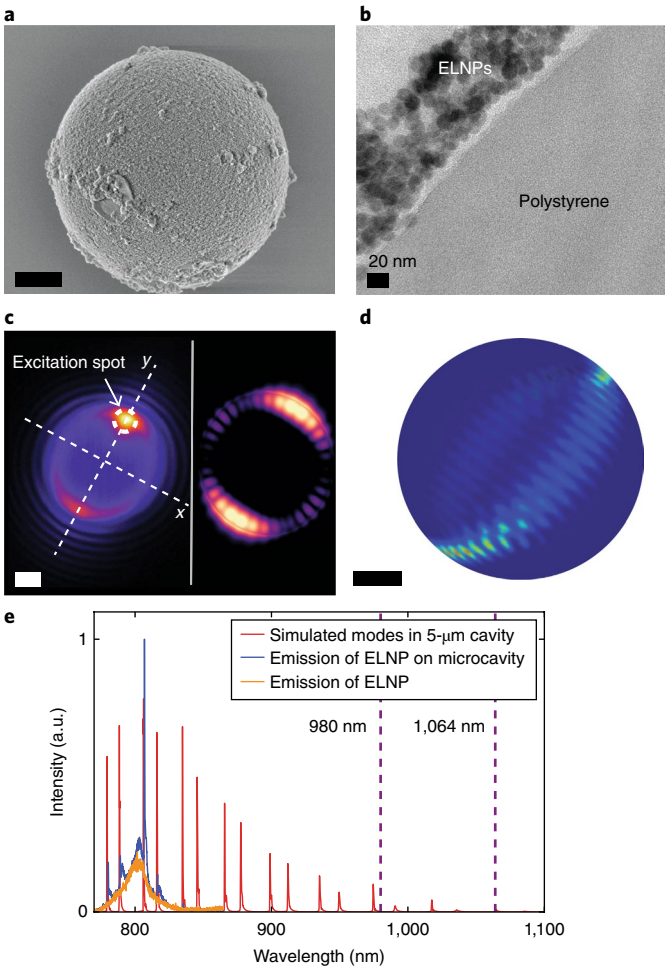

Fig. 2 | Upconverting microlaser structure and WGM properties. **a**, Scanning electron micrograph of a 5-μm-diameter polystyrene bead coated with ELNPs. **b**, Transmission electron micrograph of a cross-section of the microsphere cavity in the proximity of its equatorial plane showing that most of the nanoparticles lie on or near the outer surface of the microsphere. **c**, Left: Wide-field image of a lasing microsphere displaying optical modes circulating around the cavity. Excitation occurs at a diffraction-limited spot on the side of the bead, as marked. Right: Simulated field distributions in the *x*–*y* plane calculated for a 5-μm polystyrene microsphere, plotted in log colour scale. **d**, Representation in 3D of the numerical simulation of $|E|^2$ for the transverse magnetic WGM at 807 nm circulating around a 5-μm dielectric sphere. **e**, Simulated NIR spectra of WGMs supported by a 5-μm polystyrene microsphere, overlaid on the experimental emission spectra of ELNPs and ELNP-coated beads pumped near lasing. Scale bars, 1 μm unless otherwise indicated.

energy-looping mechanism[9] that, compared with other UCNPs, more efficiently achieves the population inversion required for lasing. These cavities are robust, showing no signs of damage or degradation under normal operating conditions (Supplementary Fig. 2).

The third essential feature of our upconverting microcavities is the controlled deposition of hydrophobic ELNPs on the outer surface of the polystyrene microspheres (Fig. 2 and Supplementary Fig. 3). As illustrated by a finite-element method simulation of the electric field intensity $|E|^2$ of an equatorial transverse magnetic WGM at 807 nm (Fig. 2d, Supplementary Fig. 4), this design maximizes the overlap of the ELNP gain medium with the cavity optical WGMs. ELNPs were deposited on the surface of the 5-μm polystyrene microspheres by partial swelling of microspheres in a polar solvent mixture to drive van der Waals interactions between hydrophobic surfaces on the ELNP and the outer region of the microsphere, followed by deswelling. Using this solution-phase process, the thickness of the ELNP coating is tuned by adjusting ELNP and microsphere concentrations (Fig. 2a,b, Supplementary Fig. 5). Transmission electron microscope cross-sections demonstrate that most of the nanoparticles form a halo on or near the outer surface of the microsphere, with few particles embedded deeper within the polystyrene matrix (Fig. 2b).

Optical images of emission from the microspheres under 1,064-nm illumination (Fig. 2c, left) match the simulated WGM spatial distribution (Fig. 2c, right, and Fig. 2d). Spectrally, the observed NIR emission modes match simulated optical mode positions for a 5-μm-diameter polystyrene bead (Fig. 2e), confirming both the size of the cavity and its effective coupling to the ELNP emission

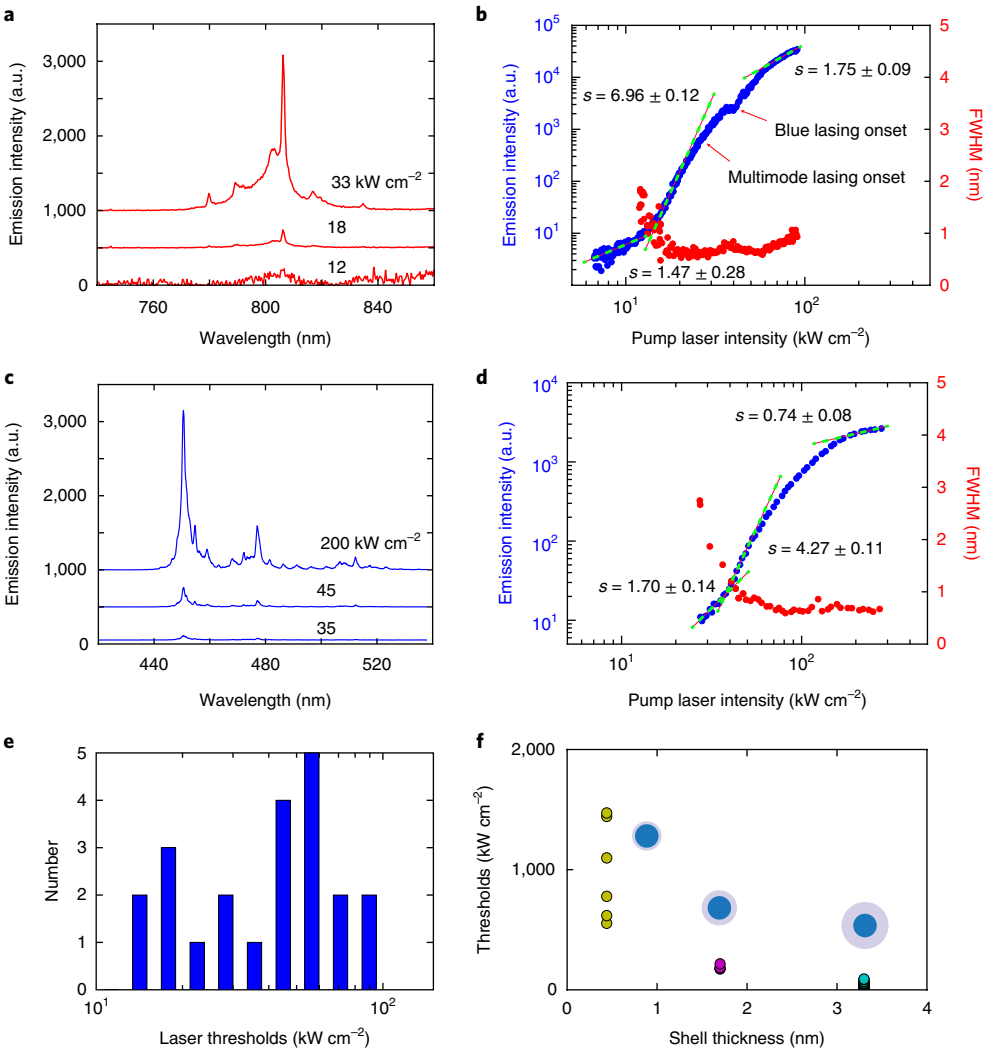

Fig. 3 | Upconverting microlaser characterization. a, NIR spectra for pump laser intensities below, near and above the lasing threshold. Spectra are offset for clarity. **b**, Microcavity emission intensity and spectral linewidth from the main NIR lasing mode at 807 nm as a function of pump intensity. FWHM, full width at half maximum. *s*, the slope to a power-law fit on a log–log plot. **c**, Blue emission spectra for pump laser intensities below, near and above the blue lasing threshold. Spectra are offset for clarity. **d**, Emission and mode linewidth versus pump intensity for the lasing mode at 450 nm. **e**, Lasing threshold distribution for 22 microspheres with near-optimal coatings, as determined by systematic electron microscopy and optical studies of ELNP compositions and coating thicknesses. **f**, Influence of epitaxial $NaGdF_4$ nanocrystal shells (illustrated by blue/grey spheres) on laser thresholds. Shell thicknesses measured by transmission electron microscope: 0.4, 1.7 and 3.3 nm (all values ±0.2 nm).

near 800 nm. Experimental *Q*-factors for these ELNP-coated microspheres range from 10^3 to 10^4 (Supplementary Fig. 6). Both transverse electric and transverse magnetic modes are present, and their relative intensities can be controlled by adjusting the input coupling position of the pumping laser (Supplementary Fig. 7).

Lasing is observed from these ELNP microcavities when the CW 1,064-nm pump laser intensity is raised above a threshold value. This value is determined by plotting both microcavity output power and spectral linewidth narrowing as a function of pump power and noting where the simultaneous change in slope occurs for both quantities (Supplementary Fig. 8). For the representative device highlighted in Fig. 3a,b, we determined that the 807-nm laser mode dominates the spectrum when the pump laser is focused at the edge of the microsphere (Supplementary Figs. 9 and 10). The exact input coupling efficiency of the pump laser is difficult to determine in this configuration, so to provide the most conservative estimate of the lasing threshold, we assume that 100% of the excitation (in a diffraction-limited spot) couples to the WGM for all thresholds listed, thus providing upper bounds for the lasing thresholds. Emission spectra from the luminescence band at approximately 800 nm for pump powers below, near and above threshold (Fig. 3a) show that cavity modes from the microsphere modify the ELNP spontaneous emission even at low pump powers. Above the threshold, a primary lasing mode at around 807 nm emerges, narrowing and increasing in relative intensity (Supplementary Fig. 8). The full emission intensity versus pump intensity curve for this mode (Fig. 3b) overlaid on its intensity-dependent linewidth plot shows a lasing threshold of 17 kW cm^{-2}. Beyond the lasing threshold, the mode linewidth narrows to <1 nm (see Supplementary Methods). Also present in Fig. 3b are slope-change features corresponding to the onset of multimode lasing and the onset of the blue lasing (Fig. 3c,d). Demonstrating the robustness of this microcavity design and its fabrication, lasing was achieved in each of the 114 microresonators tested. A distribution of lasing thresholds—observed for the 22 measured devices that were produced with optimal ELNP and coating specifications (Fig. 3e and Supplementary Fig. 10)—shows thresholds as low as 14 kW cm^{-2} and a mean value of 44 kW cm^{-2} with a standard deviation of 23 kW cm^{-2}. Previous

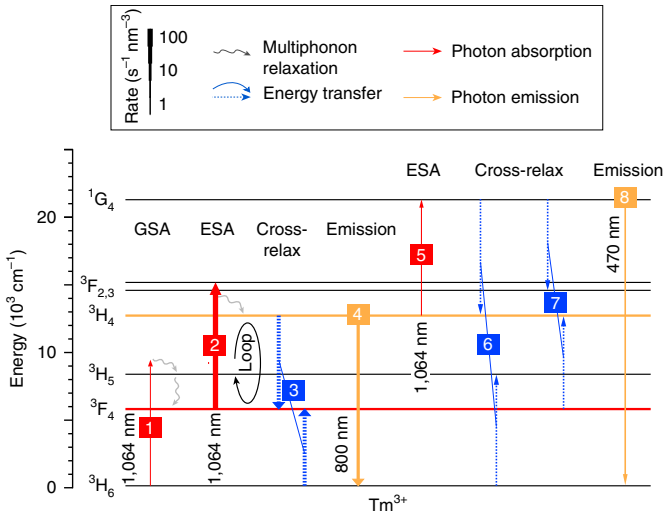

Fig. 4 | ELNP energy transfer and emission mechanisms. Looping mechanism in Tm^{3+}-doped $NaYF_4$. Energy levels represent $4f^{12}$ manifolds of Tm^{3+}. Arrows are manifold-to-manifold transitions as described in the key. The thickness of the arrows 1–5 varies logarithmically with the rate of the steady-state transitions at 1,064 nm excitation (10^5 W cm^{-2}). The thicknesses of arrows 6–8 have been enhanced for clarity. GSA, ground-state absorption.

UCNP lasing systems excited at 980 nm exhibited peak-intensity pumping thresholds of about 10^{10} W cm^{-2} with Yb^{3+},Er^{3+}-codoped UCNPs[5], and about 10^7 W cm^{-2} with Yb^{3+},Tm^{3+}-codoped UCNPs[6]. Unlike the complex pulse sequences required to avoid thermal damage with these high power densities[5,6], the low lasing thresholds in our upconverting microcavities enable excitation with modest CW lasers.

As the pump fluence is increased beyond the NIR lasing threshold, we also observe simultaneous CW blue lasing action from these microcavities (Fig. 3c,d). This lasing originates from the $^1D_2 \rightarrow {}^3F_4$ and $^1G_4 \rightarrow {}^3H_6$ transitions in Tm^{3+}, which are populated by additional excited-state absorption events (for example, from the NIR lasing $^3H_4$ state to the high-energy $^1G_4$ state; see Fig. 4). When the pump excitation power is increased near the blue lasing threshold, multiple cavity modes emerge from the spontaneous emission bands near 450 nm and 475 nm (Fig. 3c). The blue lasing thresholds are two- to tenfold greater than the NIR lasing thresholds in these systems, as can be seen in the output power versus pump intensity curve for a representative microsphere laser (Fig. 3d).

Notably, the use of optically inactive $NaGdF_4$ shells on our ELNPs is required for achieving the low-threshold CW lasing observed here. These shells prevent energy loss to the ELNP surface[22], thereby reducing an important loss channel within the microlasers and hence lowering the threshold (Supplementary Fig. 11). A single monolayer (0.4 ± 0.2 nm) shell on each ELNP only partially passivates ELNP surface losses, leading to NIR lasing thresholds ranging from 550 to 1,500 kW cm^{-2} in measured devices (Fig. 3f). Slightly thicker shells (1.7 ± 0.2 nm) lower the observed thresholds to about 200 kW cm^{-2}, and even thicker (3.3 ± 0.2 nm) shells yield even lower thresholds of about 50 kW cm^{-2} (Fig. 3f).

Based on the above observations, we conclude that the low thresholds of these microlasers are a consequence of using Tm^{3+}-doped core–shell nanoparticles that exploit the avalanche-like energy-looping mechanism[9] (Fig. 4), along with the spatial overlap of the ELNPs with microcavity WGMs. The looping mechanism amplifies the population of excited states such as $^3F_4$ through a positive feedback loop of excited-state absorption (ESA) from an intermediate state followed by cross-relaxation back down to the same intermediate state (steps 2 and 3 in Fig. 4, respectively). In this cross-relaxation process, a highly excited Tm^{3+} ion transfers a fraction of its energy to a neighbouring Tm^{3+} ion in its ground state, resulting in two Tm^{3+} ions in the same intermediate excited state. This looping process effectively doubles the population of an excited state, and repeated looping therefore can amplify the population of excited states nonlinearly. This process ultimately leads to population inversion in the $^3H_4$ state, which is responsible for the 800-nm-band emission. Once the $^3H_4$ excited state is sufficiently populated, additional ESA events are possible, including a 1,064-nm-resonant transition to the $^1G_4$ state (step 5, Fig. 4) responsible for blue emission and, in these ELNP-coated microcavities, blue lasing. These ESA events may be coupled to numerous cross-relaxation processes (steps 6 and 7, Fig. 4), thereby producing additional loops that amplify the populations of higher excited states.

Several compelling and diverse applications for these stand-alone microlasers, including in vivo biosensing[23] and deep-tissue optogenetics[24], require operation in demanding aqueous environments. We are able to observe lasing action when the microcavities are immersed in fetal bovine serum (FBS; Fig. 5a–c), demonstrating the viability of our devices in biological media (Fig. 5b). NIR microcavity emission spectra of microspheres immersed in FBS when pumped below, near and above threshold (Fig. 5c) exhibit in situ CW lasing thresholds of about 250 kW cm^{-2} (Supplementary Fig. 8); these increased thresholds are expected because of the smaller refractive index (n) contrast between the cavity and the environment. The change in environment also produced observable spectral shifts of the lasing modes ($\Delta\lambda = 2.1$ nm, Fig. 5b), indicating utility in sensing applications. More generally, the small footprint, low CW lasing thresholds and solution-processability enable integrated photonics applications[25], such as self-assembly into phased arrays for increased optical directionality or active waveguiding (Fig. 5d and Supplementary Fig. 15).

Beyond reporting on local index or material changes in the environment, more sophisticated applications can be foreseen. For example, these microlasers can potentially respond to small changes in temperature[26] or pressure—critical information from the biological perspective—owing to the sensitivity of the lasing modes to cavity shape and size. Temperature measurements can be easily calibrated using mode shifts ($\Delta\lambda$; Fig. 5e)[26]. We have measured the total increase in temperature due to lasing action in biological media to be 0.38 °C as pump laser intensity is increased from just above threshold to 1,051 kW cm^{-2} (Fig. 5f), presenting a minimal impact for biological media and tissue. For devices in air, pumped at approximately 200 kW cm^{-2}, we observe an increase of <2 °C (Supplementary Fig. 12). Notably, the intensity and wavelength of the CW lasing is stable over 5 h of continuous excitation at 300 kW cm^{-2} (Fig. 5g and Supplementary Fig. 13). In contrast, CW lasers based on semiconductor nanoparticles destabilize in less than 1 h under considerably lower fluences[10,27]. As bright, stable and local light sources, energy-looping microlasers enable subcellular imaging, tracking and probing (Supplementary Fig. 14 and Supplementary Video 1). Manipulation and trapping (both optical and thermal)[28] of small particles and molecules such as proteins and DNA are also possible.

In conclusion, we have demonstrated CW UCNP lasing in 5-μm microcavities at thresholds as low as 14 kW cm^{-2}. These upconverting microlasers, based on fully solution-processed colloidal assemblies of energy-looping nanoparticles, present a viable solution for small, stand-alone coherent light sources. Their ease of fabrication, storage and deposition combined with their ability to operate continuously for hours in liquids and biological media immediately allows the realization of new in vivo imaging, sensing and probing measurements at depths well below sample surfaces, required for optogenetic and similar investigations. With these properties, we expect UCNP microlasers to lead to photonic architectures that have until now been precluded by laser design and material constraints.

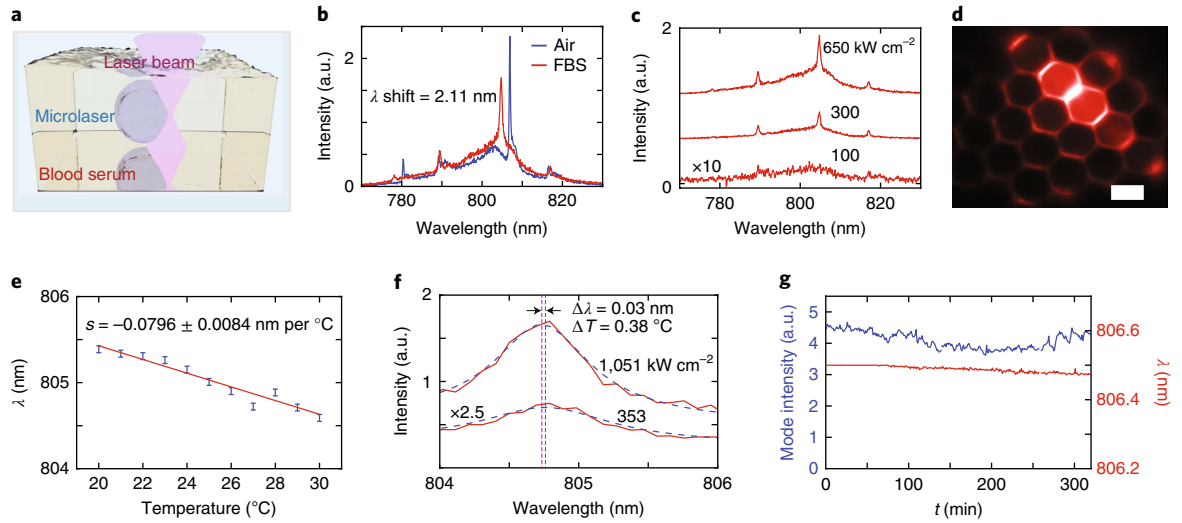

Fig. 5 | Lasing in aqueous environments, temperature sensing calibration, characterization of microlaser temperature versus pump power, and evaluation of laser stability. a, Schematic showing microlaser excitation in blood serum. **b**, Spectral shifts recorded for the lasing beads in air and blood serum. **c**, NIR spectra for pump laser intensities below, near and above the lasing threshold with the bead submerged in serum. **d**, Wide-field image of upconverting microlasers in a self-assembled 2D array; scale bar is 5 µm. **e**, Mode spectral shifts as a function of temperature (for $T = 20$–30 °C); s, the slope of the linear fit, in units of nm per °C. Error bars were determined from measured room-temperature variations and standard deviations of average spectra. **f**, Spectra of the main laser mode at two input powers for a microlaser in blood serum. $\Delta\lambda = 0.03$ nm as pump intensity is increased from 353 kW cm^{-2} to 1,051 kW cm^{-2}. Using the calibration curve in **e**, this translates to a ΔT in serum of 0.38 °C for this change in pump intensity. The blue dotted lines are peak fits. Vertical lines indicate the centre wavelength of the fitted mode. **g**, Intensity and wavelength of the laser mode over a period of 5 h under an excitation power of 300 kW cm^{-2}, displaying intensity variations below 15% and wavelength shifts less than 0.025 nm.

Data Availability. The data that support the plots and other findings within this paper are available from the corresponding authors upon reasonable request.

Received: 6 October 2017; Accepted: 3 May 2018;
Published online: 18 June 2018

References

1. Hill, M. T. & Gather, M. C. Advances in small lasers. *Nat. Photon.* **8**, 908–918 (2014).
2. Moss, D. J., Morandotti, R., Gaeta, A. L. & Lipson, M. New CMOS-compatible platforms based on silicon nitride and Hydex for nonlinear optics. *Nat. Photon.* **7**, 597–607 (2013).
3. Kim, T.-i et al. Injectable, cellular-scale optoelectronics with applications for wireless optogenetics. *Science* **340**, 211–216 (2013).
4. Jin, L. M., Chen, X., Siu, C. K., Wang, F. & Yu, S. F. Enhancing multiphoton upconversion from NaYF4:Yb/Tm@NaYF4 core–shell nanoparticles via the use of laser cavity. *ACS Nano* **11**, 843–849 (2016).
5. Zhu, H. et al. Amplified spontaneous emission and lasing from lanthanide-doped up-conversion nanocrystals. *ACS Nano* **7**, 11420–11426 (2013).
6. Chen, X. et al. Confining energy migration in upconversion nanoparticles towards deep ultraviolet lasing. *Nat. Commun.* **7**, 1–6 (2016).
7. Li, M. et al. Ultralow-threshold multiphoton-pumped lasing from colloidal nanoplatelets in solution. *Nat. Commun.* **6**, 8513 (2015).
8. Zhou, B., Shi, B., Jin, D. & Liu, X. Controlling upconversion nanocrystals for emerging applications. *Nat. Nanotech.* **10**, 924–936 (2015).
9. Levy, E. S. et al. Energy-looping nanoparticles: harnessing excited-state absorption for deep-tissue imaging. *ACS Nano* **10**, 8423–8433 (2016).
10. Grim, J. Q. et al. Continuous-wave biexciton lasing at room temperature using solution-processed quantum wells. *Nat. Nanotech.* **9**, 891–895 (2014).
11. Wu, S. et al. Non-blinking and photostable upconverted luminescence from single lanthanide-doped nanocrystals. *Proc. Natl Acad. Sci. USA* **106**, 10917–10921 (2009).
12. Dexter, D. L. Possibility of luminescent quantum yields greater than unity. *Phys. Rev.* **108**, 630–633 (1957).
13. Ovsyakin, V. V. & Feofilov, P. P. Cooperative sensitization of luminescence in crystals activated with rare earth ions. *JETP Lett. Engl.* **4**, 317–318 (1966).
14. Gargas, D. J. et al. Engineering bright sub-10-nm upconverting nanocrystals for single-molecule imaging. *Nat. Nanotech.* **9**, 300–305 (2014).
15. Johnson, L. F. & Guggenheim, H. J. Infrared-pumped visible laser. *Appl. Phys. Lett.* **19**, 44–47 (1971).
16. Grubb, S. G., Bennett, K. W., Cannon, R. S. & Humer, W. F. CW room-temperature blue upconversion fibre laser. *Electron. Lett.* **28**, 1243–1244 (1992).
17. Xie, P. & Gosnell, T. R. Room-temperature upconversion fiber laser tunable in the red, orange, green, and blue spectral regions. *Opt. Lett.* **20**, 1014–1016 (1995).
18. Bunzli, J.-C. G. & Piguet, C. Taking advantage of luminescent lanthanide ions. *Chem. Soc. Rev.* **34**, 1048–1077 (2005).
19. Strutt, J. W. B. R. *The Theory of Sound* 2nd edn, revised and enlarged (Macmillan, London, 1894).
20. Fujiwara, H. & Sasaki, K. Upconversion lasing of a thulium-ion-doped fluorozirconate glass microsphere. *J. Appl. Phys.* **86**, 2385–2388 (1999).
21. Scotognella, F., Monguzzi, A., Meinardi, F. & Tubino, R. DFB laser action in a flexible fully plastic multilayer. *Phys. Chem. Chem. Phys.* **12**, 337–340 (2010).
22. Chen, G., Qiu, H., Prasad, P. N. & Chen, X. Upconversion nanoparticles: design, nanochemistry, and applications in theranostics. *Chem. Rev.* **114**, 5161–5214 (2014).
23. Idris, N. M. et al. In vivo photodynamic therapy using upconversion nanoparticles as remote-controlled nanotransducers. *Nat. Med.* **18**, 1580–1585 (2012).
24. Wu, X. et al. Dye-sensitized core/active shell upconversion nanoparticles for optogenetics and bioimaging applications. *ACS Nano* **10**, 1060–1066 (2016).
25. Niu, W. et al. 3-Dimensional photonic crystal surface enhanced upconversion emission for improved near-infrared photoresponse. *Nanoscale* **6**, 817–824 (2014).
26. Ioppolo, T. & Manzo, M. Dome-shaped whispering gallery mode laser for remote wall temperature sensing. *Appl. Opt.* **53**, 5065 (2014).
27. Fan, F. et al. Continuous-wave lasing in colloidal quantum dot solids enabled by facet-selective epitaxy. *Nature* **544**, 75–79 (2017).
28. Yang, A. H. J. et al. Optical manipulation of nanoparticles and biomolecules in sub-wavelength slot waveguides. *Nature* **457**, 71–75 (2009).
29. Funk, D. S., Eden, J. G., Osinski, J. S. & Lu, B. Green, holmium-doped upconversion fibre laser pumped by red semiconductor laser. *Electron. Lett.* **33**, 1958–1960 (1997).
30. Sanders, S., Waarts, R. G., Mehuys, D. G. & Welch, D. F. Laser diode pumped 106 mW blue upconversion fiber laser. *Appl. Phys. Lett.* **67**, 1815–1817 (1995).
31. Dennis, M. L., Dixon, J. W. & Aggarwal, I. High power upconversion lasing at 810 nm, in Tm-ZBLAN fibre. *Electron. Lett.* **30**, 136–137 (1994).

32. Xing, G. et al. Ultralow-threshold two-photon pumped amplified spontaneous emission and lasing from seeded CdSe/CdS nanorod heterostructures. *ACS Nano* **6**, 10835–10844 (2012).
33. Yu, J. et al. Confinement of pyridinium hemicyanine dye within an anionic metal–organic framework for two-photon-pumped lasing. *Nat. Commun.* **4**, 1–7 (2013).
34. He, G. S., Bhawalkar, J. D., Zhao, C. F., Park, C. K. & Prasad, P. N. Two-photon-pumped cavity lasing in a dye-solution-filled hollow-fiber system. *Opt. Lett.* **20**, 2393–2395 (1995).
35. Fan, H. H., Guo, L., Li, K. F., Wong, M. S. & Cheah, K. W. Exceptionally strong multiphoton-excited blue photoluminescence and lasing from ladder-type oligo(*p*-phenylene)s. *J. Am. Chem. Soc.* **134**, 7297–7300 (2012).

Acknowledgements

The authors thank E. Wong for technical support. This work was performed at the Molecular Foundry and was supported by the Office of Science, Office of Basic Energy Sciences, of the US Department of Energy under contract no. DE-AC02-05CH11231. This research was in part funded under the target program no. 0115PK03029 "NU-Berkeley strategic initiative in warm-dense matter, advanced materials and energy sources for 2014-2018" from the Ministry of Education and Science of the Republic of Kazakhstan. Portions of this research were supported by the Global Research Laboratory (GRL) Program through the National Research Foundation of Korea (NRF) funded by the Ministry of Science and ICT (no. 2016911815).

Author contributions

The scientific concepts, ideas and experimental designs were the result of interactions and discussions between A.F.B., N.J.B., E.S.L, L.M., F.S., B.E.C., P.J.S. and E.M.C. E.M.C., E.S.L, C.A.T. and B.T. synthesized the nanoparticles, and A.F.B., E.S.L., L.M., B.E.C. and E.M.C. fabricated the microlasers. A.F.B., K.Y., E.S.B, N.J.B., E.S.L., L.M. and F.S. conducted the spectroscopic measurements. K.Y., K.B. and E.M.C. performed the theoretical modelling. M.V.A., A.F.B. and S.A. conducted the electron microscopy. A.F.B., B.E.C., E.M.C. and P.J.S. wrote the paper, in coordination with all the authors.

Competing interests

The authors declare no competing interests.

Additional information

Supplementary information is available for this paper at https://doi.org/10.1038/s41565-018-0161-8.

Reprints and permissions information is available at www.nature.com/reprints.

Correspondence and requests for materials should be addressed to B.E.C. or E.M.C. or P.J.S.

Publisher's note: Springer Nature remains neutral with regard to jurisdictional claims in published maps and institutional affiliations.